

Moment analysis of the Hodgkin–Huxley system with additive noise

Henry C. Tuckwell*, Jürgen Jost

Max Planck Institute for Mathematics in the Sciences, Inselstr. 22, 04103 Leipzig, Germany

ARTICLE INFO

Article history:

Received 11 March 2009

Received in revised form 19 May 2009

Available online 23 June 2009

Keywords:

Hodgkin–Huxley neuron
Stochastic processes
Moment equations

ABSTRACT

We consider a classical space-clamped Hodgkin–Huxley (HH) model neuron stimulated by a current which has a mean μ together with additive Gaussian white noise of amplitude σ . A system of 14 deterministic first-order nonlinear differential equations is derived for the first- and second-order moments (means, variances and covariances) of the voltage, V , and the subsidiary variables n , m and h . The system of equations is integrated numerically with a fourth-order Runge–Kutta method. As long as the variances as determined by these deterministic equations remain small, the latter accurately approximate the first- and second-order moments of the stochastic Hodgkin–Huxley system describing spiking neurons. On the other hand, for certain values of μ , when rhythmic spiking is inhibited by larger amplitude noise, the solutions of the moment equation strongly overestimate the moments of the voltage. A more refined analysis of the nature of such irregularities leads to precise insights about the effects of noise on the Hodgkin–Huxley system. For suitable values of μ which enable rhythmic spiking, we analyze, by numerical examples from both simulation and solutions of the moment equations, the three factors which tend to promote its cessation, namely, the increasing variance, the nature and shape of the basins of attraction of the limit cycle and stable equilibrium point and the speed of the process.

© 2009 Elsevier B.V. All rights reserved.

1. Introduction

The electrophysiological activity of single neurons has long been considered as being stochastic in nature [3,23]. The latter reference and Ref. [17] contain historical reviews; see also Ref. [8]. One underlying cause is the apparent randomness with which inputs arrive at a neuron's synapses which is often modeled by Poisson point processes or smoothed versions which are usually taken to be Gaussian white noise or processes obtained from it. There have been numerous publications in the past several years reporting the effects of noise on (usually) pyramidal cells in the cerebral cortex and other brain structures, see for example references [27,28,5,1]. To explain various aspects of the apparently random spiking of neurons, a large variety of models and methods for their analysis has been explored. These began with simple diffusion models involving Ornstein–Uhlenbeck processes ([10,2]; see Ref. [23] for historical references). More realistic stochastic point models such as that of Hodgkin–Huxley [15] were later explored by, amongst others, [22,29,7,6,26]. The analysis of such nonlinear stochastic models is complicated and standard methods from Markov process theory with Fokker–Planck or Kolmogorov equations become unwieldy.

We recently reported on our investigations of the effects of noise on the repetitive firing activity of coupled type 1 neurons [11,12]. More recently we have explored stochastic effects on single Hodgkin–Huxley model neurons undergoing periodic firing [13,24]. The results obtained by simulation showed that near the bifurcation to periodic firing, a small amount of noise could effectively silence a neuron. Furthermore, a minimum in the firing activity occurred as the noise amplitude increased, a phenomenon which we called inverse stochastic resonance. The silencing of rhythmic neural activity was verified experimentally [19] and was unexpected because most previous studies had indicated that noise usually led to

* Corresponding author.

E-mail addresses: tuckwell@mis.mpg.de (H.C. Tuckwell), jost@mis.mpg.de (J. Jost).

greater firing rates and that sometimes a maximum in the response occurs as the noise increased, a phenomenon called stochastic resonance.

When a Hodgkin–Huxley neuron is stimulated by an additive (or conductance-based) noisy current for long time periods and the mean driving current is above the critical value at which a bifurcation to periodic firing occurs and in the range of bistability, then the system may make transitions to and from the state in which the neuron is silent to the spiking state. It remains in either state a random length of time and we have considered, without much detail, the use of first-exit time theory to understand how such transitions arise [24]. In the current article we attempt to understand how small noise can drive the Hodgkin–Huxley system so easily from a state of periodic (or near-periodic) firing to the neighbourhood of a non-spiking equilibrium state and hence terminate the spiking activity. We investigate the use of the moment method which had been explored briefly in our investigations of coupled type 1 neurons [11,12]. Hence we derive the differential equations satisfied by the first- and second-order moments of the four Hodgkin–Huxley variables; such equations are given explicitly as they may be useful in investigations of other stimulating currents and different parameter values and initial conditions to those employed in the present work. Additional analysis is performed in Section 6.

2. The HH equations with additive (current) noise

The standard HH system consists of four ordinary differential equations for the electrical potential $V(t)$, the potassium activation variable $n(t)$, the sodium activation variable $m(t)$ and the sodium inactivation variable $h(t)$. The latter three variables take values in $[0, 1]$ and their differential equations involve the coefficients $\alpha_n, \beta_n, \alpha_m, \beta_m, \alpha_h, \beta_h$, all of which have dependencies on V which were obtained by approximating experimental data. For convenience we let the variables be $X_1 = V, X_2 = n, X_3 = m$ and $X_4 = h$ and we put \mathbf{X} as the vector with these components. The means of the components are denoted by $m_i, i = 1, \dots, 4$, and the second-order moments by $C_{ij}, i, j = 1, \dots, 4$. Also we denote the derivatives of $\alpha_n(V)$ etc. by α'_n . The vector of means is denoted by \mathbf{m} .

The Hodgkin–Huxley system with additive noise is thus

$$dX_1 = \frac{1}{C} [(\mu + \bar{g}_K X_2^4 (V_K - X_1) + \bar{g}_{Na} X_3^3 X_4 (V_{Na} - X_1) + g_L (V_L - X_1)) dt + \sigma dW],$$

which we abbreviate to

$$dX_1 = f_1(\mathbf{X})dt + \frac{\sigma}{C}dW \tag{1}$$

and

$$dX_2 = f_2(\mathbf{X})dt = [\alpha_n(X_1)(1 - X_2) - \beta_n(X_1)X_2] dt \tag{2}$$

$$dX_3 = f_3(\mathbf{X})dt = [\alpha_m(X_1)(1 - X_3) - \beta_m(X_1)X_3] dt \tag{3}$$

$$dX_4 = f_4(\mathbf{X})dt = [\alpha_h(X_1)(1 - X_4) - \beta_h(X_1)X_4] dt. \tag{4}$$

We will first find the 14 deterministic ordinary differential equations for the first- and second-order moments of the 4 variables in the Hodgkin–Huxley model with an additive noisy current using the approach of Rodriguez and Tuckwell [20]. Although the moment equations for the HH system were explored in a preliminary way for other purposes in Ref. [21], the equations were not given explicitly, so we have given them in the present article. The method, or extensions of it, has been employed in several recent studies of neuronal networks [4,14,18].

3. Differential equations for the first- and second-order moments of a general dynamical system

We consider firstly the general n -component diffusion process $\mathbf{X} = \{\mathbf{X}(t), t \geq 0\}$ where the j th component satisfies the stochastic differential equation

$$dX_j(t) = f_j(\mathbf{X}(t), t)dt + \sum_{k=1}^m g_{jk}(\mathbf{X}(t), t)dW_k(t). \tag{5}$$

Here the W_k 's are independent standard (zero mean, variance t at time t) Wiener processes and it is assumed that conditions for existence and uniqueness of solutions are met [9]. If the f_j 's and g_{jk} 's possess second derivatives, we find that for relatively small noise terms the means $\mu_j(t) = E[X_j(t)]$ and covariances $K_{ij}(t) = E[(X_i(t) - \mu_i(t))(X_j(t) - \mu_j(t))]$ may be approximated by the functions $m_j(t)$ and $C_{ij}(t)$ respectively. These quantities are found to satisfy the following systems of ordinary differential equations

$$\frac{dm_i}{dt} = f_i(\mathbf{m}, t) + \frac{1}{2} \sum_{l=1}^n \sum_{p=1}^n \left\{ \frac{\partial^2 f_i}{\partial x_l \partial x_p} \right\}_{(\mathbf{m}, t)} C_{lp} \tag{6}$$

$$\begin{aligned} \frac{dC_{ij}}{dt} = & \sum_{k=1}^m \{g_{ik}g_{jk}\}_{(\mathbf{m}, t)} + \sum_{l=1}^n \left\{ \frac{\partial f_i}{\partial x_l} \right\}_{(\mathbf{m}, t)} C_{lj} + \sum_{l=1}^n \left\{ \frac{\partial f_j}{\partial x_l} \right\}_{(\mathbf{m}, t)} C_{il} \\ & + \frac{1}{2} \sum_{k=1}^m \sum_{l=1}^n \sum_{p=1}^n \left\{ g_{jk} \frac{\partial^2 g_{ik}}{\partial x_l \partial x_p} + \frac{\partial g_{ik}}{\partial x_l} \frac{\partial g_{jk}}{\partial x_p} + \frac{\partial g_{ik}}{\partial x_p} \frac{\partial g_{jk}}{\partial x_l} + g_{ik} \frac{\partial^2 g_{jk}}{\partial x_l \partial x_p} \right\}_{(\mathbf{m}, t)} C_{lp}. \end{aligned} \tag{7}$$

Note that in the last equation the misplaced bracket in Ref. [20] has been corrected and a rearrangement has been effected. Also, when the noise is additive, the g_{jk} 's do not depend on the x_j 's so that the term in (7) involving the triple sum disappears and the equation is considerably simpler.

4. Application to the HH system with additive noise

We apply the preceding results to the HH system.

4.1. The means

From Eq. (6), evaluating the required partial derivatives of f_1, \dots, f_4 , we obtain the following differential equations for the means m_1, \dots, m_4 , of V, n, m, h , respectively.

$$\begin{aligned} \frac{dm_1}{dt} &= \frac{1}{C} [\mu + \bar{g}_K m_2^4 (V_K - m_1) + \bar{g}_{Na} m_3^3 m_4 (V_{Na} - m_1) + g_L (V_L - m_1) - 4\bar{g}_K m_2^3 C_{12} - 3\bar{g}_{Na} m_3^2 m_4 C_{13} - \bar{g}_{Na} m_3^3 C_{14} \\ &\quad + 6\bar{g}_K m_2^2 (V_K - m_1) C_{22} + 3\bar{g}_{Na} m_3 m_4 (V_{Na} - m_1) C_{33} + 3\bar{g}_{Na} m_3^2 (V_{Na} - m_1) C_{34}] \\ \frac{dm_2}{dt} &= \alpha_n(m_1)(1 - m_2) - \beta_n(m_1)m_2 + \frac{1}{2} (\alpha_n''(m_1)(1 - m_2) - \beta_n''(m_1)m_2) C_{11} - (\alpha_n'(m_1) + \beta_n'(m_1)) C_{12} \\ \frac{dm_3}{dt} &= \alpha_m(m_1)(1 - m_3) - \beta_m(m_1)m_3 + \frac{1}{2} (\alpha_m''(m_1)(1 - m_3) - \beta_m''(m_1)m_3) C_{11} - (\alpha_m'(m_1) + \beta_m'(m_1)) C_{13} \\ \frac{dm_4}{dt} &= \alpha_h(m_1)(1 - m_4) - \beta_h(m_1)m_4 + \frac{1}{2} (\alpha_h''(m_1)(1 - m_4) - \beta_h''(m_1)m_4) C_{11} - (\alpha_h'(m_1) + \beta_h'(m_1)) C_{14}. \end{aligned}$$

4.2. The variances

For the HH system with additive noise the differential equations for the variances of $X_i(t)$ as obtained from Eq. (7) are given in general by, for $i = 1, \dots, 4$,

$$\frac{dC_{ii}}{dt} = 2 \sum_{l=1}^4 \left\{ \frac{\partial f_i}{\partial x_l} \right\}_{\mathbf{m}} C_{li} + \sum_{k=1}^4 \{g_{ik}^2\}_{\mathbf{m}}.$$

Substituting the appropriate derivatives and coefficients we obtain

$$\begin{aligned} \frac{dC_{11}}{dt} &= -\frac{2}{C} [\bar{g}_K m_2^4 + \bar{g}_{Na} m_3^3 m_4 + g_L] C_{11} + \frac{8}{C} \bar{g}_K m_2^3 (V_K - m_1) C_{12} \\ &\quad + \frac{6}{C} \bar{g}_{Na} m_3^2 m_4 (V_{Na} - m_1) C_{13} + \frac{2}{C} \bar{g}_{Na} m_3^3 (V_{Na} - m_1) C_{14} + \left(\frac{\sigma}{C}\right)^2 \\ \frac{dC_{22}}{dt} &= 2 [(\alpha_n'(m_1)(1 - m_2) - \beta_n'(m_1)m_2) C_{12} - (\alpha_n(m_1) + \beta_n(m_1)) C_{22}] \\ \frac{dC_{33}}{dt} &= 2 [(\alpha_m'(m_1)(1 - m_3) - \beta_m'(m_1)m_3) C_{13} - (\alpha_m(m_1) + \beta_m(m_1)) C_{33}] \\ \frac{dC_{44}}{dt} &= 2 [(\alpha_h'(m_1)(1 - m_4) - \beta_h'(m_1)m_4) C_{14} - (\alpha_h(m_1) + \beta_h(m_1)) C_{44}]. \end{aligned}$$

4.3. The remaining covariances

It is seen from Eq. (7) that in general the covariances satisfy the equations

$$\frac{dC_{ij}}{dt} = \sum_{l=1}^4 \left\{ \frac{\partial f_i}{\partial x_l} \right\}_{\mathbf{m}} C_{lj} + \sum_{l=1}^4 \left\{ \frac{\partial f_j}{\partial x_l} \right\}_{\mathbf{m}} C_{il} + \sum_{k=1}^4 \{g_{ik}g_{jk}\}_{\mathbf{m}}.$$

The remaining 6 covariances for the HH system are thus found to be solutions of the following differential equations.

$$\begin{aligned} \frac{dC_{12}}{dt} &= [\alpha_n'(m_1)(1 - m_2) - \beta_n'(m_1)m_2] C_{11} - \left[\frac{1}{C} (\bar{g}_K m_2^4 + \bar{g}_{Na} m_3^3 m_4 + g_L) + \alpha_n(m_1) + \beta_n(m_1) \right] C_{12} \\ &\quad + \frac{4}{C} \bar{g}_K m_2^3 (V_K - m_1) C_{22} + \frac{3}{C} \bar{g}_{Na} m_3^2 m_4 (V_{Na} - m_1) C_{23} + \frac{1}{C} \bar{g}_{Na} m_3^3 (V_{Na} - m_1) C_{24} \\ \frac{dC_{13}}{dt} &= [\alpha_m'(m_1)(1 - m_3) - \beta_m'(m_1)m_3] C_{11} - \left[\frac{1}{C} (\bar{g}_K m_2^4 + \bar{g}_{Na} m_3^3 m_4 + g_L) + \alpha_m(m_1) + \beta_m(m_1) \right] C_{13} \\ &\quad + \frac{4}{C} \bar{g}_K m_2^3 (V_K - m_1) C_{23} + \frac{3}{C} \bar{g}_{Na} m_3^2 m_4 (V_{Na} - m_1) C_{33} + \frac{1}{C} \bar{g}_{Na} m_3^3 (V_{Na} - m_1) C_{34} \end{aligned}$$

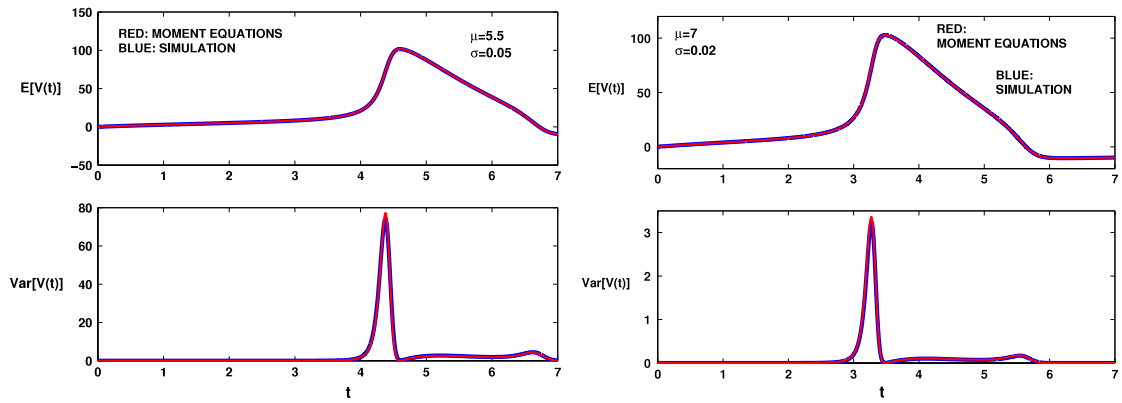


Fig. 1. Showing the excellent agreement of the mean and variance of the voltage determined by simulation (red curves) and by solving the differential equations for the moments (blue curves) for the Hodgkin–Huxley model neuron subject to small additive noise. On the left the input current parameters are $\mu = 5.5$ and $\sigma = 0.05$ and on the right, $\mu = 7$ and $\sigma = 0.02$. Here and in the following figures, time is in ms and voltage in mV. The two sets of results are practically indistinguishable. Note the large difference in the variance in the left and right sets of results. (For interpretation of the references to colour in this figure legend, the reader is referred to the web version of this article.)

$$\begin{aligned} \frac{dC_{14}}{dt} &= [\alpha'_h(m_1)(1 - m_4) - \beta'_h(m_1)m_4] C_{11} - \left[\frac{1}{C} (\bar{g}_K m_2^4 + \bar{g}_{Na} m_3^3 m_4 + g_L) + \alpha_h(m_1) + \beta_h(m_1) \right] C_{14} \\ &\quad + \frac{4}{C} \bar{g}_K m_2^3 (V_K - m_1) C_{24} + \frac{3}{C} \bar{g}_{Na} m_3^2 m_4 (V_{Na} - m_1) C_{34} + \frac{1}{C} \bar{g}_{Na} m_3^3 (V_{Na} - m_1) C_{44} \\ \frac{dC_{23}}{dt} &= (\alpha'_m(m_1)(1 - m_3) - \beta'_m(m_1)m_3) C_{12} + (\alpha'_n(m_1)(1 - m_2) - \beta'_n(m_1)m_2) C_{13} - (\alpha_m + \beta_m + \alpha_n + \beta_n) C_{23} \\ \frac{dC_{24}}{dt} &= (\alpha'_h(m_1)(1 - m_4) - \beta'_h(m_1)m_4) C_{12} \\ &\quad + (\alpha'_n(m_1)(1 - m_2) - \beta'_n(m_1)m_2) C_{14} - (\alpha_n(m_1) + \beta_n(m_1) + \alpha_h(m_1) + \beta_h(m_1)) C_{24} \\ \frac{dC_{34}}{dt} &= (\alpha'_h(m_1)(1 - m_4) - \beta'_h(m_1)m_4) C_{13} \\ &\quad + (\alpha'_m(m_1)(1 - m_3) - \beta'_m(m_1)m_3) C_{14} - (\alpha_m(m_1) + \beta_m(m_1) + \alpha_h(m_1) + \beta_h(m_1)) C_{34}. \end{aligned}$$

5. Results

The system of 14 nonlinear ordinary differential equations for the first- and second-order moments of the variables V , n , m and h was integrated using a standard fourth-order Runge–Kutta method with error control which is implemented in the software package Matlab. The initial conditions were the standard ones for the means $m_1(0) = 0$, $m_2(0) = 0.35$, $m_3(0) = 0.06$, $m_4(0) = 0.6$ and all second-order moments were initially set at zero. Note that by definition [15], $V = 0$ at the resting state. The calculations require the evaluation of the coefficients α_n , β_n , α_m , β_m , α_h , β_h along with their first and second derivatives which are all given in the Appendix. Some of these as functions of V , such as α_n and α_m have indeterminate forms at certain values of V which must be allowed for in their numerical determination.

5.1. Comparison of simulation and moment equation results

It was found in the first applications of the moment method to the Fitzhugh–Nagumo system [25] that for small noise amplitudes, the first- and second-order moments estimated from simulation and by solution of the differential equations were in good agreement. We compared results for these moments obtained by simulation of the system of stochastic differential equations for the HH system (1)–(4) (Euler method, 500 trials) and the differential equation method. For the first set of results a subcritical value of $\mu = 5.5$ was used with a small noise level $\sigma = 0.05$. As can be seen from the left part of Fig. 1, the results obtained by the two methods are almost identical and cannot be distinguished visually. The same level of agreement was found with the supercritical value $\mu = 7.0$ and a somewhat smaller noise level $\sigma = 0.02$, as seen in the right part of Fig. 1, although the maximum variance is 4% less using the moment method. The agreement between the results for the two disparate methods is surprisingly good considering the highly nonlinear nature of the system and the fact that one is solving a system of 14 coupled nonlinear differential equations to obtain the moments. Note that when the noise is additive, higher-order simulation schemes such as the Milstein scheme and the Runge–Kutta scheme of strong order 1 reduce to the simpler Euler scheme employed here [16].

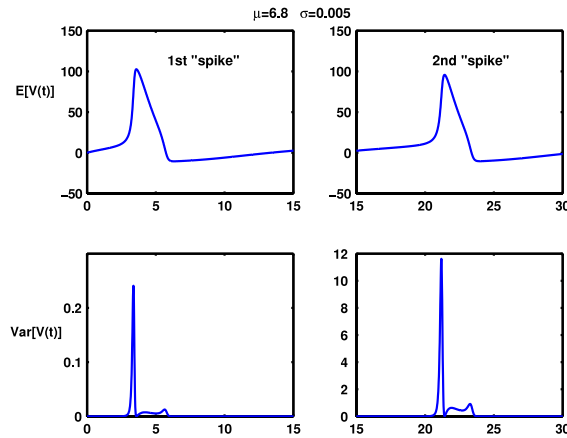


Fig. 2. Showing how in this example, with $\mu = 6.8$ and $\sigma = 0.005$, the variance (here shown for V) on the first spike is relatively small but on the second spike it is much larger. For appropriate parameter values such increases may be sufficient to drive the system off the limit cycle. See also Fig. 7.

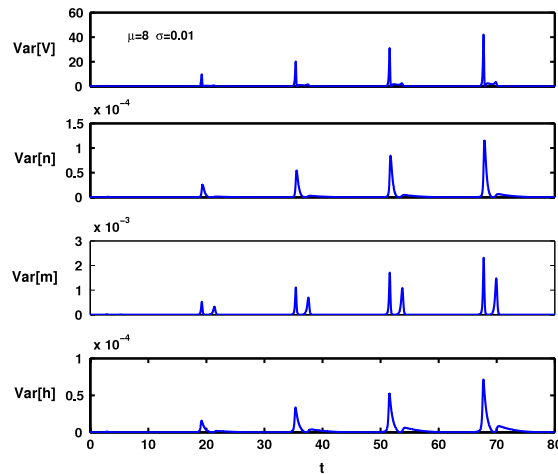


Fig. 3. Here with $\mu = 8$ and a small noise $\sigma = 0.01$ the variances of each component grow on each orbit. Eventually the variances become extremely large or the system of equations for the moments becomes unstable.

5.2. The behaviour of the variance

As can be seen from the examples of Fig. 1, it is noteworthy that the maxima in the variances of the voltage and other variables (see Fig. 3) occur quite high up on the leading edge of the spikes. Thus in the first example the maximum occurs when $V \approx 70$ mV and in the second example when $V \approx 75$ mV, which values can be compared with the peak mean value $V \approx 105$ mV. In both cases the variance has a small secondary maximum at the end of the spike when V has reached hyperpolarized states.

In Fig. 2 are shown the mean and variance of the voltage variable as determined by the solution of the differential equations for the moments when μ is just greater than the critical value at $\mu = 6.8$ and the noise is very small, at $\sigma = 0.005$. On the first orbit the process stays with a large probability close to the deterministic solution; this can be seen from the fact that the variance has a maximum value of ≈ 0.25 (compared to 0.23 by simulation). On the second spike however the variance reaches a maximum value ≈ 11.75 (10.2 by simulation) which is about 50 times as large as on the first spike. The larger variance on the second orbit increases the probability that the process switches from the spiking mode and goes to the stable equilibrium point, corresponding to a silent non-spiking cell. This is elaborated on in Section 6. Furthermore, if the solutions of the moment equations remain well-behaved, the variances grow on each orbit as is seen in Fig. 3 for $\mu = 8$ and $\sigma = 0.01$. Here the variances of all 4 components, V , n , m and h are shown as functions of time until $t = 80$. Altogether there are 5 “spikes”, as indicated by peaks in the mean voltage (not shown), the first spike having a peak variance of only 0.468 which cannot be detected in the figure. The maximal variances obtained near each spike by the moment method with corresponding values from simulation with only 500 trials in brackets are here 0.45 (0.49), 9.6 (10.1), 20.2 (19.4), 30.5 (28.0) and 41.5 (37.6). Thus here the growing variance is mainly a dynamical system property rather than an indicator that

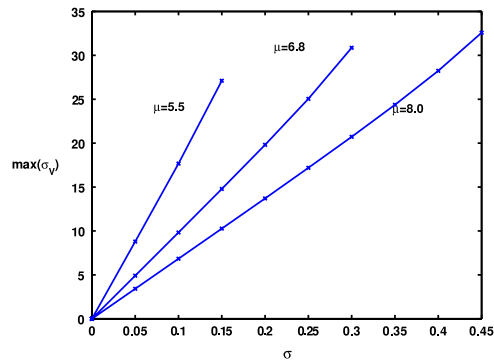


Fig. 4. The maximum standard deviation of the voltage achieved in the period to $t = 10$ for various μ as indicated, plotted against the amplitude of the input noise. The curves, which are almost linear, are terminated when the moment method breaks down.

the moment method is becoming unstable. Notice too that around each “spike” the variances of all four components have secondary peaks, which in the case of the auxiliary variables seem well separated from the earlier main peaks.

5.3. The range of validity of the moment method

In the general scheme of Section 3, the derivation of the differential equations for the moments depends on the assumption that the noise is relatively small, in order to justify the neglect of moments of the process of higher order than the third (the 3rd moment is assumed to be negligible by symmetry). Clearly when the external noise is large one would not expect the differential equation method to lead to accurate estimates of the means and second-order moments. We have seen for example that the cases shown in Fig. 1 resulted in a successful application of the moment method. The question arises in any application of the moment method as to what range of external noise amplitudes will result in satisfactory results. An exhaustive numerical investigation is not feasible here, but we can give some illustrative examples.

5.3.1. The range of σ values

The differential equations were integrated over a relatively short time period to $t = 10$ for various values of μ and σ . For small times the solutions are invariably well-behaved, but after a few or several orbits, the system becomes unstable, resulting in an extremely large numerical value for the variance. The larger the value of σ for a given μ the sooner the unstable behaviour occurs. These phenomena are indicated in Fig. 4 where the maximum standard deviation of V in its time domain of stability is plotted against σ for the three values of μ , one being subcritical (5.5), one being just supercritical (6.8) and one being well above critical (8.0). Each curve is roughly linear and has been stopped when the value of σ is reached at which the system became unstable. For $\mu = 5.5, 6.8$ and 8.0 , the respective values of σ at which the moment method breaks down are approximately 0.15, 0.3 and 0.45. The slope of the curves decreases as μ increases, reflecting the more deterministic behaviour of the system. A direct comparison of simulation and moment method results is shown in Fig. 5 where the mean and the variance are given to $t = 7$ for $\mu = 6.8$ and various σ . For $\sigma = 0.05$ both the mean and variance calculated by both methods are close; when $\sigma = 0.25$ the means are close but the moment method overestimates the variance; and when $\sigma = 0.3495$ the mean and variance given by the moment method are both inaccurate.

5.3.2. Probability distributions

In order to examine the role of the distributions of the process at various times, simulations were performed for the parameters given in Fig. 5, top and bottom sets, where agreement between moment method and simulation was excellent for $\sigma = 0.05$ and bad for $\sigma = 0.3495$. In Fig. 6 histograms are given of V and n (2000 trials) at the times corresponding to half-way up the spike $t = 3.25$ and after the spike $t = 4.5$. In the small noise case the distributions meet fairly well the conditions required in deriving the moment equations as they are symmetric and fairly well concentrated about the means. The third and fourth central moments (to powers 1/3 and 1/4) were suitably small relative to the mean. However, for the larger value 0.3495 of σ the distribution of V at $t = 3.25$ is not at all symmetric, and is concentrated at larger values. The distribution of n is also strongly skewed at this epoch.

For $t = 4.5$, the distribution of V is quite symmetric but that of n is still skewed. Furthermore, even for small σ , the distribution of V on the falling edge of the spike is not symmetric (not shown), being bunched up at larger values, reflecting the fact that there is an upper limit for V which acts in the fashion of a reflecting or natural barrier. This property seems to be a manifestation of the very sharp peak of the Hodgkin–Huxley spike with these parameter values. However, the time spent by the process near the peak is small which may explain why the moment method is accurate despite the fact that a condition used in its derivation is not met.

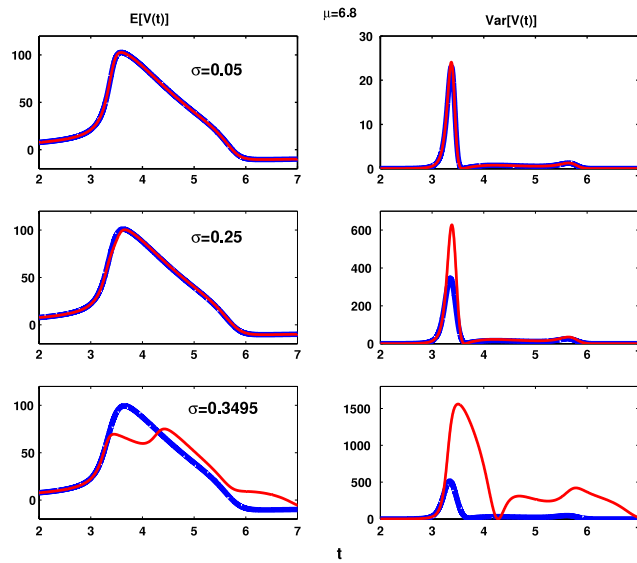


Fig. 5. The mean and variance as functions of time as determined by the moment method (red curves) and by simulation (blue curves) for $\mu = 6.8$ and various σ . It can be seen that the agreement between results obtained by simulation and the moment method becomes progressively worse as σ increases. (For interpretation of the references to colour in this figure legend, the reader is referred to the web version of this article.)

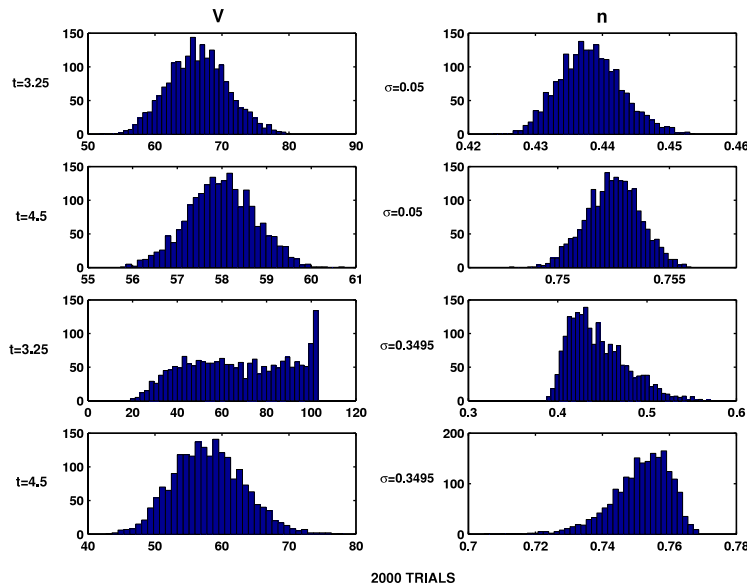


Fig. 6. Histograms of V (left column) and n (right column) from simulations (2000 trials) of the HH system with $\mu = 6.8$ and two values, small and large of the noise parameter σ . For each σ the distributions are shown at the times $t = 3.25$ and $t = 4.5$. Compare these times with the results of Fig. 5.

6. The termination of rhythmic spiking

It is of interest to investigate the factors involved in the termination of rhythmic spiking by noise and the occurrence of minima in firing rate which have been principally found to occur for values of μ not far above the bifurcation value $\mu_c \approx 6.4$ [13,24]. The factors which seem most relevant are (1) the variance of the process (2) the size and shape of the basin of attraction of the (spiking) limit cycle (3) the speed of the process at the relevant parts of the orbit. We briefly explore each of these factors in turn.

6.1. The variance of the process

Noise of a very small amplitude, for example $\sigma < 0.05$, usually has little effect on the spiking activity of the HH model, even for those values of μ where termination of spiking may be readily induced by larger values of $\sigma \approx 0.5$. It is desirable

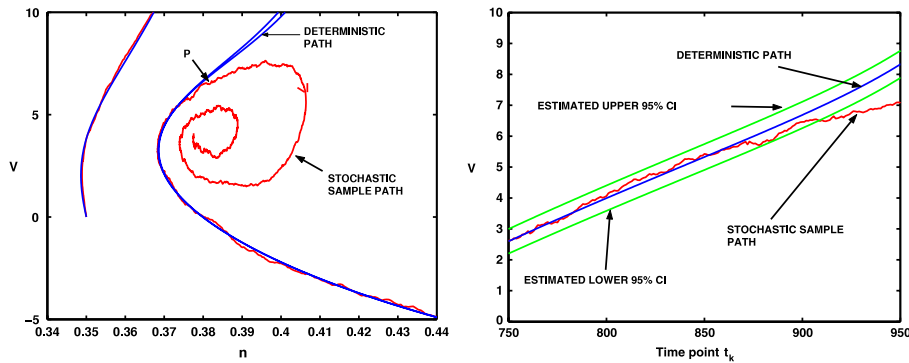


Fig. 7. Left: Here is shown a noise-driven exit on the second spike from spiking to stable equilibrium point. The deterministic orbits are shown in blue. Parameter values $\mu = 6.8$, $\sigma = 0.25$. The point marked P is approximately the exit point. Right: An expanded view of the departure from spiking. Also shown are the values of $V(t) \pm 95\%$ confidence intervals using the variance of V obtained by the solving the moment differential equations. (For interpretation of the references to colour in this figure legend, the reader is referred to the web version of this article.)

to ascertain the magnitude of the variance at various parts of the orbits to see what role it has in the persistence or not of the spiking state. However, the moment method does not give much information about the variance when σ is larger than the limiting values depicted in Fig. 4. Whereas the moment method is useful for small noise, which for some μ can stop rhythmic firing, the minima in firing rate occur at values of σ (around 0.4 and 0.5) where the moment method is not valid. Simulation may always be used to estimate the variance of the process but this needs an exceedingly large number of trials to obtain usefully small confidence intervals for variables of interest. Simulation also has the less serious drawback of some uncertainty in quantities determined through random number generators.

Nevertheless, we are able to make some progress as follows. The left part of Fig. 7 shows a part of the deterministic spiking activity (blue curves) of an HH neuron for $\mu = 6.8$ and for stochastic activity (red curves) with the same μ and $\sigma = 0.25$. With these parameters it is found that of order one trial in ten results in termination of spiking on the second or third spike. In the figure, spiking terminates on the second spike and the sample path can be seen to collapse to the stable equilibrium point not far from rest. The moment method does remain stable up to the leading edge of the second spike and hence the variance can be estimated at the part of the orbit where the path leaves the basin of attraction of the limit cycle. In the right part of Fig. 7 are shown the 95% confidence intervals (green curves) obtained by using the variance from the solution of the moment equations and the deterministic orbit, again depicted by the blue curve. The stochastic path stays fairly close to the deterministic orbit and within the confidence intervals until it swings downward to the lower one. It does not escape here but a short time later it does. Thus, the variance, as indicated by the confidence limits, is indeed a factor in the escape of the process from the basin of attraction of the limit cycle.

6.2. The geometry of the basin of attraction of the limit cycle

The basins of attraction of the limit cycle (for supra-threshold values of μ) and of the stable equilibrium point are not known exactly. Numerical investigations may be used to obtain a heuristic idea of the size and location of the basin of attraction of the limit cycle by examining the simulated paths of the process to see where (approximately) they depart from their trajectories close to the limit cycle. This was done for $\mu = 6.7$ and $\sigma = 0.4$, for 40 cases where noise induced the termination of spiking. Although the process is four-dimensional, it is sufficient here to consider just the n and V components as the variations in m and h at the exit points are relatively small.

The results are shown in Fig. 8, where the diamonds indicate approximate exit points (n_e, V_e) . It can be seen that the range of values of n_e is very small, being between 0.368 and 0.424. Similarly the exit points have values of V_e between 3.56 and 9.37. The mean values are $E[n_e] = 0.396$ and $E[V_e] = 6.57$ with standard deviations of 0.0127 and 1.41 respectively. The histograms of values were approximately symmetric and approximately Gaussian. It is seen that the values of (n_e, V_e) where the process escapes occupy a fairly small region of (n, V) -space. Outside this region near both the inside and outside of the spike trajectory the process tends not to escape from the limit cycle attractor. Thus it seems that near this small region the basin of attraction of the limit cycle is quite narrow, making it relatively easy for the process to move to the equilibrium point and hence terminate the spiking. To obtain more insight, we determined the approximate basin of attraction of the stable equilibrium point. Since 4 dimensions are hard to represent, we determined asymptotic (large time) behaviours of solutions at $29 \times 41 = 1189$ grid points over the rectangle $V \in [3, 10]$, $n \in [0.35, 0.45]$. Since in the portion of phase space of interest, m and h do not change rapidly, we used their average values 0.1346 and 0.4572, respectively. The results are shown in Fig. 9, where the dark blue area shows the regions where points acting as initial data led to the stable equilibrium point without spiking. This figure, which can be compared with Fig. 8, gives an approximation to the basin of attraction of the stable equilibrium point. It can be seen that the limit cycle solution passes close to this region, which explains why a relatively small perturbation from it would lead to the cessation of spiking, until noise might drive the system back up to

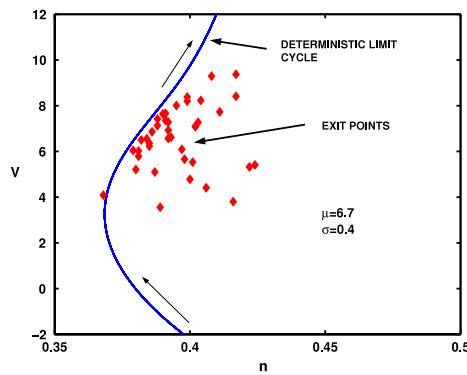


Fig. 8. Showing the approximate locations in the (n, V) -plane where the stochastic trajectories depart sufficiently from the deterministic trajectory to terminate the spiking. Here $\mu = 6.7$ and $\sigma = 0.4$. 40 points are plotted.

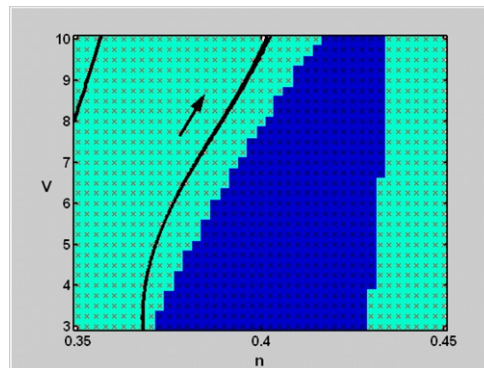


Fig. 9. Here is shown the calculated *approximate* basin of attraction of the stable equilibrium point (dark blue) in relation to the limit cycle solution (marked with arrow) without noise for $\mu = 6.7$. Compare this with the exit points with noise shown in Fig. 8. (For interpretation of the references to colour in this figure legend, the reader is referred to the web version of this article.)

the basin of attraction of the limit cycle. It seems however by inspection of Fig. 8 that the actual basin of attraction of the equilibrium point extends to regions closer in (n, V) -space to the limit cycle than the approximation shown in Fig. 9.

6.3. The speed of the process

It is of interest to determine the speed of the process as it traverses the limit cycle or in the random case as it traverses paths near the limit cycle. For the deterministic case ($\sigma = 0$) the speed is a non-random process and given by

$$u(t) = \left(\sum_{i=1}^4 \left[\frac{dx_i}{dt} \right]^2 \right)^{1/2},$$

where x_1, x_2, x_3 and x_4 are the (noise free) voltage and auxiliary variables. The same formula can be applied to the stochastic case, but that now the components and the speed U are random processes and technically the derivatives do not exist.

It is hypothesized that the variations in speed at various parts of the limit cycle is a contributing factor to the termination of regular spiking activity by noise. In Fig. 10 we show the speed plotted against time along with values of V , the voltage, and n , the potassium activation variable. On the right-hand set of results, the speed is shown near the mean exit point for cases indicated in the previous figure. It is seen that relative to the maximum speed v_{max} in orbit, as the process passes by the region where exits from the basin of attraction of the limit cycle are most likely, the speed is only about $0.006 v_{max}$, lending support to the idea that a very small speed contributes to the collapse away from the limit cycle.

7. Conclusions

The moment differential equation method has been found useful for analyzing the effects of noise in the Fitzhugh–Nagumo [25] and other neurodynamical systems [4,14,18]. Our recent studies of the HH neuron subjected to noisy inputs, especially with regard to inhibitory effects, led us to its application in that framework. We have here explored the use of the moment method for the Hodgkin–Huxley system with additive (current) Gaussian white noise. The set of 14

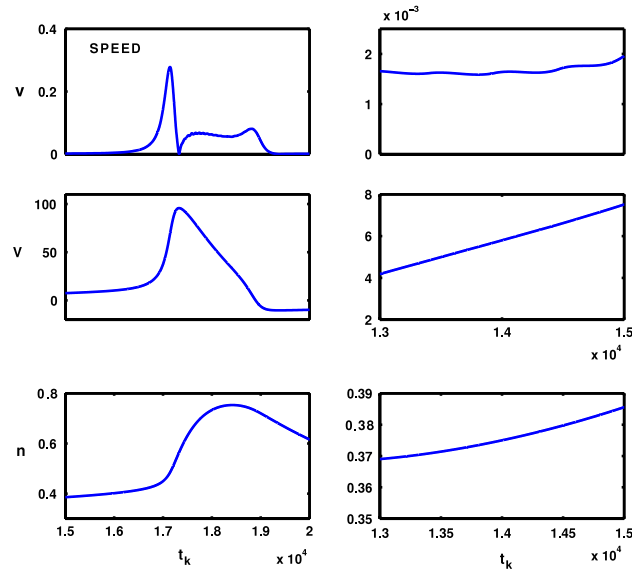


Fig. 10. The speed v , potential V and potassium activation n plotted against time. On the right-hand set of results the parts of the trajectories are shown expanded close to the mean exit point.

differential equations for the first- and second-order moments was given explicitly and solved using standard numerical methods. The moments compared favourably with those obtained by simulation when the noise was small, and the range of σ values for which agreement was good was, as anticipated, larger the larger the mean input μ .

A phenomenon of interest is the recently found silencing of rhythmic spiking of neurons by noise, which runs counter to the usual positive effects of stochasticity on firing rates. The greatest such impacts of noise had been found for μ near the critical value (about 6.4) and for values of σ in the range 0.2–0.8. The moment method is only stable for short time periods with these parameter values and hence we have resorted to a combination of moment method and simulation to investigate the factors involved in the termination of rhythmic spiking. However, we have considered the case of a continuously applied stimulus whereby the variance continues to grow and the moment method eventually breaks down. In the case of intermittent stimuli, the moment method is expected to perform better over wider ranges of noisiness of the input.

Appendix. HH coefficients and their derivatives

Recalling that here V is depolarization and not membrane potential (cf. the original forms in HH (1952)), the coefficients in the auxiliary equations are the following standard ones.

$$\alpha_n(V) = \frac{10 - V}{100[e^{(10-V)/10} - 1]}, \quad \beta_n(V) = \frac{1}{8}e^{-V/80}$$

$$\alpha_m(V) = \frac{25 - V}{10[e^{(25-V)/10} - 1]}, \quad \beta_m(V) = 4e^{-V/18}$$

$$\alpha_h(V) = \frac{7}{100}e^{-V/20}, \quad \beta_h(V) = \frac{1}{e^{(30-V)/10} + 1}.$$

In the moment equations we require their first- and second-order derivatives. The latter are

$$\alpha'_n(V) = \frac{10 - Ve^{1-\frac{V}{10}}}{1000 \left(e^{1-\frac{V}{10}} - 1 \right)^2}$$

$$\beta'_n(V) = -\frac{1}{640}e^{-V/80}$$

$$\alpha'_m(V) = \frac{10 + e^{\frac{25-V}{10}}(15 - V)}{100 \left(e^{\frac{25-V}{10}} - 1 \right)^2}$$

$$\beta'_m(V) = -\frac{2}{9}e^{-V/18}$$

$$\alpha'_h(V) = -\frac{7}{2000}e^{-V/20}$$

$$\beta'_h(V) = \frac{e^{\frac{30-V}{10}}}{10\left(e^{\frac{30-V}{10}} + 1\right)^2}.$$

The corresponding second derivatives are found to be

$$\alpha''_n(V) = \frac{2\beta[(10 - \beta V) - 5(\beta e - 1)(1 - V/10)]}{10^4(\beta e - 1)^3}$$

$$\beta''_n(V) = \frac{1}{51200}e^{-V/80}$$

$$\alpha''_m(V) = \frac{2\alpha(\alpha(15 - V) + 10) - 10e^{-\frac{V}{10}}(25 - V)(\alpha - 1)}{1000(\alpha - 1)^3}$$

$$\beta''_m(V) = \frac{1}{81}e^{-V/18}$$

$$\alpha''_h(V) = \frac{7}{40000}e^{-V/20}$$

$$\beta''_h(V) = \frac{\gamma}{100}\left(\frac{1}{(1 + \gamma)^2} + \gamma\right)$$

where

$$\alpha = e^{\frac{25-V}{10}}$$

$$\beta = e^{-\frac{V}{10}}$$

$$\gamma = e^{\frac{30-V}{10}}.$$

References

- [1] M. Badoual, M. Rudolph, Z. Piwkowska, et al., *Neurocomputing* (65–66) (2005) 493.
- [2] A.N. Burkitt, *Biol. Cybern.* 95 (2006) 1.
- [3] B.D. Burns, A.C. Webb, *Proc. R. Soc. Lond. B* 194 (1976) 211.
- [4] G. Deco, D. Marti, *Phys. Rev. E* 75 (2007) 031913.
- [5] A. Destexhe, M. Rudolph, J.-M. Fellous, et al., *Neuroscience* 107 (2001) 13.
- [6] J.-F. Feng, D. Brown, J. Comput. Neurosci. 16 (2004) 237.
- [7] J.-F. Feng, G. Li, *J. Phys. A* 34 (2001) 1649.
- [8] W. Gerstner, W.M. Kistler, *Spiking Neuron Models*, Cambridge University Press, Cambridge, 2002.
- [9] I.I. Gihman, A.V. Skorohod, *Stochastic Differential Equations*, Springer, Berlin, 1972.
- [10] B. Gluss, *Bull. Math. Biophys.* 2 (1967) 233.
- [11] B.S. Gutkin, J. Jost, H.C. Tuckwell, *Europhys. Lett.* 81 (2008) 20005.
- [12] B.S. Gutkin, J. Jost, H.C. Tuckwell, *Theory Biosci.* 127 (2008) 135.
- [13] B.S. Gutkin, J. Jost, H.C. Tuckwell, *Naturwissenschaften* (2009), in press (doi:10.1007/s00114-009-0570-5).
- [14] H. Hasegawa, *Physica A* 388 (2009) 499.
- [15] A.L. Hodgkin, A.F. Huxley, *J. Physiol. (Lond.)* 117 (1952) 500.
- [16] P.E. Kloeden, E. Platen, *Stoch. Hydrology & Hydraulics* 3 (1989) 155.
- [17] B. Lindner, J. García-Ojalvo, A. Neiman, L. Schimansky-Geier, *Phys. Rep.* 392 (2004) 321.
- [18] A.C. Marreiros, et al., *NeuroImage* 44 (2009) 701.
- [19] D. Paydarfar, D.B. Forger, J.R. Clay, *J. Neurophysiol.* 96 (2006) 3338.
- [20] R. Rodriguez, H.C. Tuckwell, *Phys. Rev. E* 54 (1996) 5585.
- [21] R. Rodriguez, H.C. Tuckwell, *BioSystems* 48 (1998) 187.
- [22] H.C. Tuckwell, *J. Theoret. Neurobiol.* 5 (1986) 87.
- [23] H.C. Tuckwell, *Stochastic Processes in the Neurosciences*, SIAM, Philadelphia, 1989.
- [24] H.C. Tuckwell, J. Jost, B.S. Gutkin, 2009 (submitted for publication).
- [25] H.C. Tuckwell, R. Rodriguez, *J. Comput. Neurosci.* 5 (1998) 91.
- [26] H.C. Tuckwell, F.Y.M. Wan, *Physica A* 351 (2005) 427.
- [27] Y. Shu, A. Hasenstaub, M. Badoual, et al., *J. Neurosci.* 23 (2003) 10388.
- [28] X.-J. Wang, *J. Neurophysiol.* 79 (1998) 1549.
- [29] X. Yu, E.R. Lewis, *IEEE Trans. Biomed. Eng.* 36 (1989) 36.